A Contemporary Look at Biomechanical Models of Myocardium

Reza Avazmohammadi[1], **João S. Soares**[1,2], **David S. Li**[1], **Samarth S. Raut**[1], **Robert C. Gorman**[3], and **Michael S. Sacks**[1]

[1]James T. Willerson Center for Cardiovascular Modeling and Simulation, Oden Institute for Computational Engineering and Sciences, and Department of Biomedical Engineering, University of Texas, Austin, Texas 78712, USA

[2]Department of Mechanical and Nuclear Engineering, Virginia Commonwealth University, Richmond, Virginia 23284, USA

[3]Gorman Cardiovascular Research Group, Smilow Center for Translational Research, Perelman School of Medicine, University of Pennsylvania, Philadelphia, Pennsylvania 19104, USA

Abstract

Understanding and predicting the mechanical behavior of myocardium under healthy and pathophysiological conditions are vital to developing novel cardiac therapies and promoting personalized interventions. Within the past 30 years, various constitutive models have been proposed for the passive mechanical behavior of myocardium. These models cover a broad range of mathematical forms, microstructural observations, and specific test conditions to which they are fitted. We present a critical review of these models, covering both phenomenological and structural approaches, and their relations to the underlying structure and function of myocardium. We further explore the experimental and numerical techniques used to identify the model parameters. Next, we provide a brief overview of continuum-level electromechanical models of myocardium, with a focus on the methods used to integrate the active and passive components of myocardial behavior. We conclude by pointing to future directions in the areas of optimal form as well as new approaches for constitutive modeling of myocardium.

1. INTRODUCTION

Myocardium is the muscular tissue of the heart, possessing distinctive physiological, mechanical, microstructural, and electrical characteristics, and is a paradigm of functional efficiency. Heart failure (HF) typically occurs when the myocardium fails, becoming too

stiff and not allowing enough blood to fill the ventricles during diastole, too dilated and not contracting properly during systole to meet ejection fraction demands, or regionally malfunctional due to the acute injury from lack of oxygen and infarction (1). Adverse effects can even occur as secondary effects due to diseased heart valves (2), pulmonary hypertension (3), bacterial or viral infections (4), cancer treatment (5), or unexpected pharmacological interactions (6). In the United States, HF afflicts approximately 6 million people, costs $34.4 billion each year, and continues to be the single most common diagnosis for individuals older than 65 (7). Because myocardium undergoes significant structural and biomechanical changes in patients with heart disease (1, 8, 9), a better understanding of myocardial biomechanics will reveal more details of the underlying pathophysiologies of disease, improve clinical treatment, and advance medical device design.

Clinical treatment of cardiac disease may involve changes in diet and lifestyle, reduction of risk factors, medication, and surgical intervention. Interventions include pacemaker leads mounted on the tissue, stents deployed to prop open narrowed or blocked blood vessels that deliver blood to the myocardium, cardiac ablation or resection performed to improve electrical properties, or injectable biomaterials introduced to alter the mechanical behavior of the failing tissue (10). In each of these cases that involves physical interactions between devices and tissues, modeling and simulation that incorporate biomechanical mechanisms play a vital role in determining the optimal designs of the devices and procedures. In essence, such designs depend on the critical link between the organ-level cardiac function and the behavior of the tissue at smaller scales (down to molecular levels) that could be provided by myocardium models.

As in many biomedical applications, the development of biomechanical models of myocardium relies on appropriate characterization of the structure–function relationship at the tissue level. As is the case for many other soft fibrous tissues, the major steps in determining a concise and robust constitutive model for the mechanical behavior of myocardium include (*a*) delineating its general characteristics, (*b*) establishing a consistent mathematical framework, (*c*) identifying a specific functional form that contains sufficient information to represent the three-dimensional (3D) mechanical properties and microstructure of the tissue, (*d*) conducting efficient model parameter estimation using designed experiments, and finally (*e*) evaluating the predictive capability of the model (11–13).

Here, we review fundamental concepts relevant to the understanding and modeling of myocardial biomechanics. First, we provide a brief overview of myocardium structure and function, specifically myocytes, extracellular matrix (ECM), and tissue architecture. Then, we elaborate on the current constitutive approaches used in cardiac biomechanics. Finally, we review methods used to incorporate active behavior into the constitutive models.

2. MYOCARDIUM STRUCTURE AND FUNCTION

Myocardium is a very complex tissue with multiple highly interconnected length scales (Figure 1) in a well-refined structural and functional hierarchy, ranging from whole-heart biomechanics down to the basic functional unit for contraction, regulated by the actin–

myosin cross-bridge cycling mechanism (14, 15). The effective mechanical behavior of myocardium at the organ and tissue scales strongly depends on the response of its constituents and their structural arrangement at the cellular and intracellular levels. For this reason, before proceeding with biomechanical models of macroscopic behavior of myocardium, we briefly review some of the pertinent studies on its microstructural characteristics. In this section, we aim to provide a sufficient level of understanding and cognizance of the microstructural details of myocardium relevant to tissue-level mechanical modeling. We refer the interested reader to other articles that review exclusively the diverse biological, electrical, and physiological aspects of myocardium (e.g., 16–19).

2.1.   Intra- and Extracellular Composition and Structure

Myocardium is a composite tissue that makes up the walls within the heart, consisting of cardiomyocytes and fibroblasts supported by the ECM and perfused by fluid delivered by blood vessels. Cardiomyocytes (myocytes) are the primary constituent, and in the mammalian heart they can be grossly approximated as large cylindrical rods with a length-to-diameter aspect ratio of up to seven to one (20). However, myocyte sizes and shapes are diverse and influenced by species, age, and disease. Myocytes have extensive sarcomeric units, and their intracellular ionic environment is highly controlled with ion channels. A rather strong and specialized intercellular connection, the intercalated disc, connects a large number of myocytes in series in supracellular structures. In addition to the physical mechanical connection provided by the intercalated discs, myocytes are extensively connected by gap junction channels that enable propagation of action potential to control the ionic environment and trigger coordinated muscle contraction (Figure 2*a*). Intercalated discs facilitate synchronized contraction among different myocytes for end-to-end transmission of force and action potential. Connected at intercalated discs, branching and merging into one another, the myocytes form a railway-like network of myofibers in cardiac tissue (21) and dominate heart composition (22), as they occupy approximately three-fourths of the tissue volume. Cardiac fibroblasts are much smaller and more numerous than myocytes, and they play a major role in the maintenance of the ECM, which provides mechanical support and anchors both to and in between cardiomyocytes.

At the subcellular level, myocytes contain many myofibrils running in parallel along their longitudinal direction. When observed under microscope, the myofibrils reveal a distinct repeated pattern of bands. These systematic ensembles of bands form the basic functional units of the myocyte, the sarcomere, and the molecular mechanism for their contraction (Figures 1 and 2) (17). One sarcomere consists of several thick and thin filaments made of myosin and actin, respectively. Thin filaments are anchored at only one of their ends at a Z disc (with one Z disc anchoring multiple thin filaments) and run parallel to the thick filament toward the sarcomere center. Thick filaments are anchored at both ends to neighboring Z discs by the protein titin, which has exceptional elastic properties (up to 170% extension).

Actin thin filaments contain binding sites for myosin thick filaments, but at resting potential, the sites are blocked by the protein tropomyosin. Action potential changes negating the resting potential cause calcium ions (Ca^{2+}) to flow into the cell and trigger abundant Ca^{2+} release from the sarcoplasmic reticulum inside the cell. Increased Ca^{2+} facilitates binding of

Ca^{2+} to troponin C, leading to the exposure of the actin binding sites. Simultaneously, in the presence of adenosine triphosphate (ATP), energy is released, causing angular movement of these myosin heads. The myosin head binds to an adjacent position in the actin thin filament, resulting in relative sliding and generating a force that causes the sarcomere to shorten in length. This is known as the cross-bridge cycling mechanism of the sliding filament theory (Figure 2*b*). The power stroke of myosin heads causes actin to move relative to them, and the synchronous cross-bridge cycling of multiple filaments, sarcomeres, and myocytes results in effective contraction of the tissue and force propagation at the macroscopic scale.

Surrounding the myocytes and the myofibers, the ECM consists mainly of fibrillar collagen, elastin, and polyglycans (30) and is maintained by the fibroblasts in the tissue. It is composed of high-strength type I collagen (85%) and highly deformable type III collagen (15%) (31) in the form of endomysial, perimysial, and epimysial fibers. These fibers collectively form the scaffold required for supporting the myofibers and capillaries to maintain their arrangement and distribute the load across the tissue. Endomysial collagen surrounds the individual myofibers within the lamina, either as a fine weave running around the peripheral myofiber surfaces or as the transverse links connecting adjacent myocytes and often attached near Z discs (26, 32). Perimysial collagen, consisting mainly of type I collagen with high tensile strength (33), connects the adjacent laminae and also runs peripherally around a group of myofibers, bundling them together. This binding between layers is weaker near the midwall region due to longer perimysial collagen fiber lengths, allowing more freedom in comparison to subepicardium regions (25). Epimysial collagen is a sheath of connective tissue that surrounds the entire muscle (34; also see Figures 1 and 3 for graphical depictions of this arrangement).

Lastly, two main representations have been proposed to describe the arrangement and interaction of collagen and myofibers. Earlier studies by Caulfield & Borg (35), Borg & Caulfield (36), and Borg et al. (37) introduced a "strut" representation for collagen fibers, connecting myofibers to myofibers perpendicularly (Figure 3*c*). The struts were perceived to connect myofibers to capillaries as well, such that they are attached perpendicularly to capillaries but tangentially to myofibers. This representation was helpful in explaining how strained collagen links maintain the patency of the capillaries in systole, whereas the links between myofibers become stretched in diastole and maintain the diastolic arrangement of the myofiber bundles. This strut theory was endorsed by others, until Macchiarelli et al. (29) and Intrigila et al. (26), using scanning electron microscopy and reticulum-staining techniques, described collagen as arranged in sheaths surrounding myofibers (i.e., as a weave instead of individual struts) (Figure 3*b*). The sheath representation is currently prevalent; however, a coexistence of sheaths and struts seems to be a plausible arrangement, which will require more comprehensive investigation of myocardium architectures and could be used for microstructurally based constitutive modeling, as discussed in the next section.

2.2. Tissue- and Organ-Level Architecture and Function

Histologically, myocardium has been observed to be composed of long myofibers, formed by myocytes arranged along their principal axis and coupled end to end (analogous to skeletal muscle fibers). Fiber orientation smoothly rotates throughout the ventricular wall

(20) and is described with a helical angle. In addition, ventricular myocytes are organized by sheets in radial–tangential planes called myocardial laminae, each consisting of four to six layers of myocytes (Figure 4) (25). In an idealized description, these laminae at the midwall region are stacked at an angle relative to the longitudinal direction that helically varies along the radial direction. Nevertheless, this highly ordered structure is an idealization. Fiber and sheet organization is highly complex and regionally variable. There is no definite origin or termination point for myofibers; at best, they can be described as part of a 3D mesh. The relatively older approach put forward by Torrent-Guasp et al. (38) suggests an interesting helical pattern of the fibers, somewhat similar to the Gordian knot (39). In addition, the laminar structure has multiple branching points to encompass and accommodate the extracellular fibrous component of the tissue, and the ventricular wall is perfused by an extensive vascular network both between and across laminae (Figure 4) (40).

With the advent of diffusion tensor magnetic resonance imaging (DT-MRI) that can capture myofiber directions in full 3D, a tremendous amount of information has become available. Consistent with the description obtained from electron microscopy of small cuboidal specimens, DT-MRI has revealed that laminar surfaces appear roughly as twisted surfaces going across the wall and stacked from apex to base (33). Anderson et al. (27) proposed two families of fibers: one tangential to the epicardial surface and another at approximately 40° to the epicardium running across the wall thickness without any orderly arrangement of supporting fibrous tissue. Interestingly, this description of cardiac fiber structure suggests that the septum, shared by the left ventricle (LV) and the right ventricle (RV), anatomically belongs to the LV. Different dominant muscle layers in the same heart at different transmural depths have also been observed using DT-MRI (43).

The ECM and the mechanical support it provides play important roles in development, remodeling, and signaling in myocardium. The ECM maintains the structural integrity of blood vessels and myocytes and facilitates the load transfer throughout the myocardial wall during active contraction (46). The triple-helical structure of collagen is known to be relatively stiff, such that a modest fibrotic increase in collagen content following pressure overload or myocardial infarction could lead to a substantial increase in local tissue stiffness (47). In addition to the role of the ECM in the overall stiffness of myocardium, its composition is an important factor in the structural anisotropy of myocardium. For instance, the development of large forces in the cross-fiber direction in contracting myocardium (Figure 5*a*) is still puzzling, while complex architecture of the ECM is suspected to be a key contributor to this behavior (45). Additionally, the transmural variation in ECM composition leads to differences in elastic anisotropy at various myocardial depths (22, 48).

As in the body's connective tissues, the collagen fibrils in myocardium are initially coiled or crimped in a twisted configuration to enhance tensile strength at higher strains (34). Since this crimping does not initially bear load, it follows that the behavior of myocardium at low-strain regimes is governed by the myofiber response alone, whereas collagen fibers and their interactions with myofibers dominate the behavior at higher strains (Figure 5*b*). At slack length, collagen fibers of epi- and endocardium layers form a crisscross pattern, while at peak systole, the fibers become aligned along longitudinal and circumferential directions. This may be a well-designed mechanism to protect overstretching of the myocytes and

minimize the amount of shear stress sustained during systole (49). Lastly, in rat papillary muscles, Robinson et al. (34) observed elastic fibers (elastin) helically running around the myocytes. These also suggested that, during the cardiac cycle, the elastin fibers facilitate diastolic expansion by storing energy during systole.

3. BIOMECHANICS OF PASSIVE MYOCARDIUM

There has been a long-standing interest in quantifying the forces and stresses acting in the myocardium for both a fundamental understanding of cardiac mechanics and clinical implications (e.g., 50–56). Three important reasons to quantify myocardium wall stresses in health and/or disease (53) are as follows: (*a*) The wall stress determines myocardial oxygen consumption; (*b*) the renormalization of the wall stress may serve as a feedback cue for myocardial remodeling in diseases characterized by abnormal loading of the ventricles, such as pulmonary hypertension and congestive HF; and (*c*) an understanding of ventricular mechanics may lead to insights into the fundamental principles underlying the general function of the heart. Given the tremendous advances in computational modeling, quantitative knowledge of the evolving changes and adaptations over time of the ventricular stress distribution (during the cardiac cycle) can be used as a target to guide the optimal design of medical devices by virtual prototyping (57, 58), as well as the design of ventricular interventions such as hydrogel injection (59, 60).

3.1. Constitutive Modeling: The Gateway to Cardiac Function Simulation

Constitutive modeling is the development of mathematical relationships between myocardial wall kinematics (the deformations of the tissue during the cardiac cycle) and wall stresses (the localized forces acting on a continuum element of the tissue). It is currently possible to quantify ventricular wall kinematics experimentally with diverse imaging techniques. Yet, ventricular wall stresses cannot be measured directly—they must be computed through constitutive relationships. In this section, we review constitutive models developed for the passive behavior of myocardium. We focus on contemporary models that consider myocardium to exhibit nonlinear and anisotropic behavior, consistent with its fibrous structure. Also, we restrict our attention to incompressible models of myocardium, with a brief discussion of the effect of compressibility in the last section.

The mechanical behavior of myocardium is usually approached by assuming it is pseudoelastic (11) and is therefore described by a pseudoelastic stored energy density function W (61). Before describing the existing forms of W in detail, we present a brief review of the basic relevant kinematic relations and stress definitions (for further details, see, e.g., References 62 and 63).

Upon application of external loading, a material point $\mathbf{X}$ in the reference configuration of the representative tissue element moves to a new point $\mathbf{x} = \mathbf{x}(\mathbf{X}, t)$ at time t in the deformed configuration. The deformation gradient tensor $\mathbf{F} = \text{Grad } \mathbf{x}$ characterizes the deformation of the material. The right and left Cauchy–Green tensors are defined as $\mathbf{C} = \mathbf{F}^T \mathbf{F}$ and $\mathbf{B} = \mathbf{F} \mathbf{F}^T$, and the Green–Lagrange strain tensor is given by $\mathbf{E} = (\mathbf{C} - \mathbf{I})/2$, where $\mathbf{I}$ is the identity tensor. The second Piola–Kirchhoff stress tensor $\mathbf{S}$ can be described in terms of the stored energy density function W through

$$\mathbf{S} = 2\frac{\partial W}{\partial \mathbf{C}}, \quad 1.$$

and the Cauchy stress tensor is given by $\boldsymbol{\sigma} = J^{-1} \mathbf{F} \mathbf{S} \mathbf{F}^{\mathrm{T}}$, with $J = \det(\mathbf{F})$. Finally, for the case of nearly incompressible tissues, the above constitutive relation is replaced by

$$\mathbf{S} = 2\frac{\partial W}{\partial \mathbf{C}} - p\mathbf{C}^{-1}, \quad 2.$$

where p is the hydrostatic pressure and the incompressibility constraint $J = 1$ is enforced.

An established approach in constitutive modeling involves treating the tissue as a continuum and assuming that at any given point there exists both intracellular and extracellular space. This assumption implies that the variables of interest (e.g., strain and stress) are measured (or estimated) at a sufficiently large length scale in comparison to the underlying discrete structures. Within the realm of this assumption, the available models for constitutive behavior of the myocardium can be divided into two groups: phenomenological and structurally informed. We define phenomenological models as those that are based on general empirical observations of the material symmetry of the myocardium and that do not account for further specific compositional and structural information of the myocardium. In contrast, we define structurally informed models as those that contain quantitative information about the composition and microstructure of the myocardium, generally on a scale of less than 1 mm for human hearts. Both types of models are described below.

3.2. Phenomenological Constitutive Models

Phenomenological models aim to describe the lumped effects of different fibrous constituents (e.g., myo- and collagen fibers) inside a continuum element. On the basis of a chosen material symmetry, W for these models is often expressed in terms of kinematic invariants of the right Cauchy–Green deformation tensor $\mathbf{C}$. The formulation of W based on these invariants offers a wide range of forms in correspondence with the anisotropy spectrum of the tissue. In addition, physical interpretations of the kinematic invariants allow W to be specified by including each individual term to represent a constituent or reflect an underlying mechanism. In contrast, it is sometimes more convenient to express energy in terms of the components of the strain tensor $\mathbf{E}$ because it is easier to control strain components in an experimental setup than to control deformation invariants. This approach also facilitates the identification of the specific form of the energy function, provided that the available mechanical data based on the strain components sufficiently cover the kinematic space. However, when choosing specific forms of W based on components of $\mathbf{E}$, one must take extra care not to violate the principle of material frame indifference.

In the following subsections, we review both energy forms and categorize them into two classes: transversely isotropic and orthotropic models. For the sake of brevity, we describe

the general form of energy for each category; Table 1 presents the specific forms of the energy function W for phenomenological models.

3.2.1.   Invariant-based models.—To the best of our knowledge, Fuchs et al. (64) proposed the first (nonlinear) isotropic model for myocardial tissues that has the same form as the Mooney–Rivlin model used in the context of rubber elasticity (65). Also, Guccione et al. (66) studied the classical isotropic Fung model as the special case of their anisotropic model.

<u>**3.2.1.1.   Transversely isotropic.:**</u> Myocardium exhibits a strongly anisotropic behavior arising mainly from the arrangement of myofibers and the collagen network (see Section 2). Transversely isotropic models were the first phenomenological models proposed to account for the anisotropy of myocardium. Following an idealization of the microstructure, these models lump all fiber types into an effective fiber constituent, identified by the local mean fiber direction $\mathbf{f}_0$ in the reference configuration. Therefore, the energy function W takes the functional form $W = \psi(I_1, \ldots, I_5)$, where the invariants I_4 and I_5 account for the fiber contributions, defined as

$$I_4 = \mathbf{f}_0 \cdot \mathbf{C}\,\mathbf{f}_0, \quad I_5 = \mathbf{f}_0 \cdot \mathbf{C}^2\,\mathbf{f}_0. \quad 3.$$

Stored energy density functions for transversely isotropic (phenomenological) models are commonly proposed in the reduced form of $W = \psi(I_1, I_4)$—although this reduction has recently been debated (77), demonstrating the importance of the I_5 term under simple shear loading conditions. For the reduced form, the Cauchy stress tensor can be written as

$$\boldsymbol{\sigma} = -p\,\mathbf{I} + 2W_1\,\mathbf{B} + 2W_4\,\mathbf{f} \otimes \mathbf{f}, \quad 4.$$

where $\mathbf{f} = \mathbf{F}\,\mathbf{f}_0$ denotes the fiber direction in the deformed configuration, and $W_i = \partial W / \partial I_i$.

Perhaps the first phenomenological model of this form was a simple generalized Fung-type model proposed by Humphrey & Yin (67). Thereafter, more involved choices of W were proposed; these include both polynomial forms, originally proposed by Humphrey et al. (68, 78), and exponential forms, such as those put forward by Lin & Yin (45) and Kerckhoffs et al. (69). Note that these models (45, 68, 78), in addition to the individual I_1 and I_4 terms, include coupling (i.e., a term with I_1 and I_4) to account for the interactions between the ground matrix and the fibers.

<u>**3.2.1.2.   Orthotropic.:**</u> More recent histological studies of the microstructure of myocardial tissues indicate that the myocardium is a composite of layers (or sheets) of tissue separated by "cleavage planes" (see Section 2.1). Each sheet is composed of locally parallel muscle fibers in the sheet plane and is interconnected with a spatial network of collagen fibers. On the basis of this description, the microstructure of myocardium can be characterized by an orthonormal set of base vectors consisting of the unit vector $\mathbf{f}_0$, aligned with the average fiber direction (or fiber axis); the unit vector $\mathbf{s}_0$, which is in the plane of the

sheet and orthogonal to the fiber axis; and the unit vector $\mathbf{n}_0$, which is normal to the plane of the sheet. Figure 6*a* depicts the layered structure and the associated orthogonal set. In this review, we use the subscripts *f*, *s*, and *n* to denote the fiber, sheet, and normal directions, respectively.

Orthotropic phenomenological models (based on the above-mentioned description of myocardial microstructure) rely on the intuitive fact that the local effective behavior of the myocardium in the plane transverse to the fiber direction (i.e., the $\mathbf{s}_0$–$\mathbf{n}_0$ plane) is not isotropic. In the case of incompressible orthotropic materials characterized by the material directions ($\mathbf{f}_0$, $\mathbf{s}_0$, $\mathbf{n}_0$), the stored energy density function *W* takes the functional form $W = \psi(I_1, I_2, I_4, I_5, I_6, I_7)$, where I_6 and I_7 are two additional deformation invariants, defined as

$$I_6 = \mathbf{s}_0 \cdot \mathbf{C}\,\mathbf{s}_0, \quad I_7 = \mathbf{s}_0 \cdot \mathbf{C}^2\,\mathbf{s}_0. \quad 5.$$

In this case, it is useful to introduce an additional (dependent) invariant I_8, defined as (81)

$$I_8^2 = \left[\mathbf{f}_0 \cdot (\mathbf{C}\,\mathbf{s}_0)\right]^2 = I_2 + I_4 I_6 + I_5 + I_7 - I_1(I_4 + I_6). \quad 6.$$

Reduced forms of *W* for orthotropic models are commonly employed and are given by $W = \psi(I_1, I_2, I_4, I_6, I_8)$. For such a model, the Cauchy stress tensor can be written as

$$\begin{aligned}
\boldsymbol{\sigma} = {}& -p\,\mathbf{I} + 2(W_1 + I_1 W_2)\mathbf{B} - 2\,W_2\,\mathbf{B}^2 \\
& + 2\,W_4\,\mathbf{f} \otimes \mathbf{f} + 2\,W_6\,\mathbf{s} \otimes \mathbf{s} + W_8(\mathbf{f} \otimes \mathbf{s} + \mathbf{s} \otimes \mathbf{f}),
\end{aligned} \quad 7.$$

where $\mathbf{s} = \mathbf{F}\,\mathbf{s}_0$ denotes the fiber direction in the deformed configuration.

A prominent invariant-based orthotropic model was introduced by Holzapfel & Ogden (70) on the basis of the orthonormal material directions ($\mathbf{f}_0$, $\mathbf{s}_0$, $\mathbf{n}_0$). An advantage of this model over earlier transversely isotropic models is that it can put into evidence (*a*) the nonisotropic behavior of myocardium in the plane transverse to the fiber direction and (*b*) the possible interaction between the fiber and sheet directions when compared with the simple shear experimental data of Dokos et al. (79). A similar constitutive form accounting for the contribution of the myocardial behavior in the $\mathbf{n}_0$ direction was later developed (71). The energy forms consisting of (I_f, I_s), (I_f, I_n), (I_s, I_n), or (I_f, I_s, I_n) performed strikingly similarly, probably because of the interdependence between these invariants: $I_1 = I_f + I_s + I_n$.

3.2.2.   Strain component–based models.—Constitutive models developed in terms of the components of the strain tensor (E_{ij}) are remarkably useful for experimental testing systems that provide data for fitting their parameters; however, they need to satisfy the principle of material frame indifference for applicability to all other deformations.

3.2.2.1.   Transversely isotropic.: Yin et al. (72) proposed a simple Fung-type energy function for the biaxial behavior of myocardium, which consists of one exponential term as a polynomial function of strain components E_{11} and E_{22}. The axes of the test apparatus, identified by the $\mathbf{e}_1$ and $\mathbf{e}_2$ directions, were taken to be aligned with the fiber and cross-fiber directions, respectively. Although aligning the material and apparatus axes facilitates parameter identification due to the minimization of in-plane shearing, it could severely limit the kinematic space within which the fitted model can reasonably predict the tissue behavior (82, 83). This point is discussed further in Section 3.4, below. In addition, Yin et al.'s model did not include the coupling term between the behaviors in two perpendicular directions, as was later demonstrated to be important for the biaxial behavior of the right ventricular free wall (RVFW) myocardium (73, 84).

Guccione et al. (66) proposed a transversely isotropic model for the 3D behavior of myocardium. The model uses an idealized cylindrical coordinate system (f, c, r) representing fiber, cross-fiber, and radial directions and assumes that the behavior of the myocardium is the same in the cross-fiber and radial directions. The model accounts for coupling in the transverse plane, but not between the fiber and cross-fiber directions. Although subsequent experimental observations (25, 79, 85) revealed considerably orthotropic behavior of myocardium, this model offers a highly tractable implementation in organ-level finite-element simulations and has been extensively used for this purpose to date.

3.2.2.2.   Orthotropic.: The so-called pole-zero model, presented by the Hunter group (41, 74), appears to be the first 3D orthotropic strain component–based model of myocardium. This model relies on the fiber–sheet–normal description of myocardium microstructure, and its W consists of six terms corresponding to contributions of the stretch along each material direction (i.e., the $\mathbf{f}_0$, $\mathbf{s}_0$, and $\mathbf{n}_0$ axes) as well as the shearing within each material plane (i.e., $\mathbf{f}_0$–$\mathbf{s}_0$, $\mathbf{f}_0$–$\mathbf{n}_0$, and $\mathbf{s}_0$–$\mathbf{n}_0$ planes). In particular, the parameters A_{ii} (no sum) and A_{ij} ($i \neq j$) correspond to the extensional stiffness along material axes and shear stiffness in the material planes, respectively. A peculiar feature of this model is that it exhibits inextensibility at some limiting strains (or poles), characterized by the parameter B_{ij}, which can occur in both stretching and shearing. Although myocardium commonly exhibits a strong stiffening effect (but not quite inextensibility) when subjected to large-strain equibiaxial loading (45, 86), whether an exponential function can sufficiently capture such stiffening is debatable.

Costa et al. (75) proposed a generalization of the Fung-type (exponential) model by Guccione et al. (66) to an orthotropic model to distinguish between the behaviors in two cross-fiber directions. This model requires seven parameters, and its exponential stiffening is consistent with the results of simple shear tests performed by Dokos et al. (79). However, as is the case for Guccione's model (66), it is still worth investigating the necessity of including coupling terms between the stretching in the fiber and cross-fiber directions.

Finally, motivated by the simple shear experiments by Dokos et al. (79), Schmid et al. (76) adopted the fiber–sheet–normal functional form of the pole-zero model and presented new models by changing the descriptor function $a\,E^2/(b - |E|^c)$ in the pole-zero model to another function. The descriptor functions these authors proposed include the exponential form

$a\,e^{b\,E^2}$ and $a\,\mathrm{IntTan}(b\,E^2)$, where the function $\mathrm{IntTan}(x)$ denotes the Taylor series of the indefinite integral of $\tan(x)$, truncated after the fifth term. The idea behind this form is to construct a descriptor that exhibits strong-enough stiffening at large stretches but does not have an infinite slope like the pole-zero function, which is difficult (and not advisable) to implement in computational analyses.

3.3. Structurally Informed Models

The phenomenological models reviewed in the preceding section offer a quantitative tool to describe the effective behavior of the tissue without taking into account statistical information about the compositional detail and structural and material properties of the myocardium constituents. For this reason, it is difficult to precisely infer from these models the micromechanical mechanisms that involve the coupling between myocytes and collagen fiber ensembles under physiological or pathological conditions.

In contrast, structurally informed models are based on descriptors that account for compositional and microstructural details (typically on a scale of less than 1 mm), which attempt to establish a link between the effective biomechanical behavior of myocardium and the underlying mechanisms taking place at the microstructural level. In practice, because of the profound complexity of myocardium microstructure, these models are developed following appropriate idealizations.

For the case of structural models, W is usually written as the sum of the mechanical contribution of the continuous ECM and its embedded fibers, including myo- and collagen fibers:

$$W = \Psi^g(I_1) + \Psi^f(I_1) = \Psi^g(I_1) + \Psi^m(\mathbf{E}) + \Psi^c(\mathbf{E}) + \Psi^i(\mathbf{E}), \quad 8.$$

where the contribution of the ground matrix W^g is isotropic and a function of I_1. The fiber contribution ψ^f can be further split into terms describing the contributions of myofibers (m), collagen fibers (c), and the interactions between them (i), in the mechanical behavior of myocardium. Note that the mass/volume fraction for each constituent is commonly absorbed by the respective term in Equation 8. The effective energy contribution for each fiber type is the sum of the energies for all the fiber ensembles, weighted by the orientation distribution function $R(\mathbf{N})$, where $\mathbf{N}$ is a unit vector identifying the span of fiber orientation in the reference configuration. The energy function for each fiber ensemble is commonly expressed in terms of deformation only along the fiber, denoted by $w(I^f)$, where $I^f = \mathbf{N} \cdot \mathbf{C}\,\mathbf{N}$ is an invariant associated with the fiber deformation. As a result, the average of $w(I^f)$ over all the fiber ensembles in the representative tissue element Ω may be written as

$$\Psi^f = \int_\Omega R(\mathbf{N})w(I^f)d\Omega. \quad 9.$$

For the case of collagen fibers, they are known to be undulated in the zero-stress state, and given their negligible bending stiffness, they do not accommodate any applied loading until fully straightened. Thus, the actual (true) deformation in an individual fiber can be expressed as $I^t = I^f / \lambda_s^2$, where λ_s is the fiber slack stretch. With the use of a distribution function $D(\lambda_s)$ to account for the gradual recruitment of undulated fibers in a statistical sense, the energy contribution of collagen fibers can be rewritten as

$$\Psi^f = \int_\Omega R(\mathbf{N}) w^*(I^f) d\Omega = \int_\Omega R(\mathbf{N}) \int_{x=1}^{\sqrt{I^f}} D(x) w(I^t) dx \, d\Omega, \quad 10.$$

where x is a dummy variable in the stretch space of each individual fiber, and w^* is the modified energy accounting for the recruitment. Below, we review some existing structural models in chronological order (Table 2).

3.3.1. Horowitz model.—Building on the structural model by Lanir (89) for general connective tissues, Horowitz et al. (87) proposed a model that accounts for the distribution of both myo- and collagen fibers. The system of collagen fibers exhibits a "hairy" arrangement, connecting the myofibers to one another. All the fibers are assumed to behave linearly once recruited. The orientation of the fibers is described in spherical coordinates.

3.3.2. Humphrey model.—Motivated by the layered morphology of the myocardium, Humphrey & Yin (80) proposed a simple structural model that treats the heart as a layered composite, with each layer exhibiting transverse isotropy with in-plane fiber direction $\mathbf{N}$ (Figure 6*b*). An approximate linear transmural variation for the vector $\mathbf{N}$ allows the calculation of the average of $w(I^f)$ over the thickness of myocardium. However, this model does not account for distribution of fibers within each layer, and assumes that the effect of gradual recruitment of fibers is negligible ($w^* = w$). The behavior of each layer is characterized by the phenomenological energy function of Humphrey & Yin (67). Sacks & Chuong (90) later proposed a similar constitutive model for RVFW myocardium, with the modification that the model makes use of the energy form of Humphrey et al. (68) for each layer instead.

3.3.3. Hunter model.—Hunter et al. (74) proposed a structural model that accounts for the distribution of fibers about the orthogonal fiber–sheet–normal microstructural directions and makes use of the pole-zero descriptor $aE^2/(b-E)^c$ to characterize the response of all families of fibers. The energy is written as the sum of the contributions of three families of fibrous connective tissues (mainly collagen); however, the effect of gradual recruitment of fibers is assumed to be negligible. The fiber orientation within each family has a Gaussian distribution about a mean direction, which is aligned with each of the microstructural directions (i.e., $\mathbf{f}_0 = \mathbf{N}_1$, $\mathbf{s}_0 = \mathbf{N}_2$, and $\mathbf{n}_0 = \mathbf{N}_3$).

3.3.4. More recent models.—Surprisingly, the area of structural modeling of myocardium seems to have been inactive after Hunter et al.'s (74) model, until recently. This may be due to persistent difficulties in achieving a thorough quantitative characterization of

the collagenous ECM in myocardium, which has recently become more feasible through advances in imaging and image processing. For instance, Lee et al. (91) revisited the structural models by Horowitz et al. (87) and Eriksson et al. (92). Krishnamurthy et al. (93) studied the effect of fiber dispersion on myocardium active behavior. Avazmohammadi et al. (88) developed a structural model for the passive behavior of RVFW myocardium using histologically measured, 3D transmural orientation distributions for both myo- and collagen fibers. By taking advantage of these measurements, their model accounted for the contribution of both myo- and collagen fibers and the interaction among them in the mechanical behavior of myocardial tissues.

3.4.   Optimal Design of Mechanical Tests: A Critical Need

Schmid et al. (71, 76) compared different material models by using three metrics: goodness of fit, determinability, and variability. Goodness of fit is a measure of how well the model fits the data. Determinability describes how sensitive the material parameters are to disturbances in the data. Finally, variability reflects how broadly a material parameter could vary between the individual fits. However, the core approach underlying contemporary studies on evaluating myocardium material laws is limited to finding a model that best fits the existing data. To date, this approach has been prevalent in the general field of tissue characterization, which, in our opinion, reflects a disconnect between the experiments and the a posteriori chosen model. As a result, the estimated parameters may not be able to sufficiently predict the behavior of the tissue in general loading conditions (not included in the original data) and may not be stable against the presence of noise, although they provide a "best" fit to the existing data.

While the form of the model is critical for the characterization of myocardium, a reverse approach may provide more robust results (i.e., choosing an appropriate model and determining what experiments are best to quantify the model), referred to as optimal loading paths. Indeed, although a complete suboptimal set of strain paths is sufficient to quantify a 3D form of W for myocardium and to provide an excellent fit of the form to those paths, it may fall short in adequately describing the behavior of myocardium under general boundary conditions during a cardiac cycle. Along these lines, Avazmohammadi et al. (13) proposed an approach that not only is based on the full 3D kinematic space but also (more importantly) uses the theory of optimal design of experiments to determine the optimal loading paths for a given model form. These authors demonstrated that carrying out such an analysis before performing the experiment is essential to secure sufficient predictive capability and determinability of the chosen model. Such attributes were not evaluated in previous 3D studies.

3.5.   Is Fiber Structure Essential in Modeling Myocardium Mechanical Behavior?

The length scale of structural units in the myocardium, such as the collagen network and myocytes, ranges from nanometers to micrometers; thus, accurate modeling of the myocardium in sufficient detail is inherently a multiscale problem. Moreover, the structural characteristics of myocardium, such as the local orientation of the myo- and collagen fibers, are spatially heterogeneous and vary with position throughout the tissue from base to apex and from endocardium to epicardium. Therefore, the myocardium does not actually possess

structural uniformity, which is essential to define a representative tissue element for an inhomogeneous specimen (94). In practice, many experimental analyses of the mechanical behavior of the myocardium (72, 79, 95) are performed on an intermediate scale, which consists of a cubic slice from base, equator, or apex. This intermediate scale is referred to as the mesoscopic scale. In the porcine heart, a representative cubic slice typically measures 3 $\times$ 3 $\times$ 3 mm (79), but these dimensions vary depending on the size of the heart wall. Unless the structural uniformity across the cubic samples is demonstrated, it is crucial to account for the variations of the directions of the local myo- and collagen fibers to obtain an accurate characterization of myocardium (92, 96–98).

4. ELECTROMECHANICAL MODELING OF MYOCARDIUM

The formulation of cardiac electromechanics can be presented through three distinct interconnected models and their governing equations (99, 100), namely (*a*) cell model equations characterizing the transmembrane current and action potential in terms of ion concentrations, (*b*) reaction–diffusion equations characterizing the propagation of electrical excitation, and (*c*) the equations of motion of continuum mechanics. These equations are incorporated with two sets of constitutive laws: (*a*) the stress–strain relations for the passive behavior of myocardium (covered in Section 3) and (*b*) the relationship among active tension, calcium concentration, and cell kinematics (101, 102). Reviewing the latter is beyond the scope of this review; instead, we focus on the available continuum-level methods to couple the mechanically active and passive behaviors of myocardium.

There are currently three common approaches to incorporating the active contraction into the mechanics of the myocardium: (*a*) active stress, (*b*) active strain, and (*c*) Hill's three-element model. These approaches can be represented by different arrangements of passive (or spring) elements and contractile elements (Figure 7). We review each in turn below.

4.1. Active Stress

The most common approach to account for active tension in myocardial mechanics is to linearly add the forces generated by muscle contraction to the passive forces, represented by parallel spring and contractile elements (Figure 7*a*). This additive decomposition of the total stress is expressed simply as (41, 45, 103–105)

$$\mathbf{S} = \mathbf{S}^{act} + \mathbf{S}^{pas} = \mathbf{S}^{act} + 2\frac{\partial\, W^{pas}(\mathbf{F})}{\partial\, \mathbf{C}}, \quad 11.$$

where $\mathbf{S}^{act}$ and $\mathbf{S}^{pas}$ denote the active and passive parts of the total mechanical stress, respectively. In this model, both contractile and passive elements experience the same deformation (Figure 7*a*), which may not precisely represent the cross-bridge kinematics at the cellular level (Figure 2*b*).

4.2. Active Strain

A less common approach, called the active strain model (106–111), is inspired by the idea that production of active contraction is a dissipative process (unlike passive deformation,

which is fully recoverable) (112). Rather than the stress, the total deformation instead follows a multiplicative decomposition, written as $\mathbf{F} = \mathbf{F}^e \mathbf{F}^a$. The inelastic deformation $\mathbf{F}^a$ characterizes the muscle shortening, which is the result of the acto-myosin cross-bridge machinery (Figure 2b), and the elastic deformation $\mathbf{F}^e$ preserves the compatibility of the total deformation. The active contribution $\mathbf{F}^a$ needs to be constitutively provided as a function of the intracellular calcium concentration. The total stress in this case is given by

$$\mathbf{S} = 2\frac{\partial\, W(\mathbf{F}^e)}{\partial\, \mathbf{C}}. \quad 12.$$

In this approach, both contractile and passive elements experience the same stress but undergo different deformations (Figure 7b).

4.3. Hill Model

The third model, which can be considered a generalization of the two previous approaches, is inspired by the classical Hill model for excitation–contraction coupling (61, 113). This model consists of three elements (Figure 7c): one spring element and one contractile element in series (as in the active strain model), in parallel with another spring element (as in the active stress model). Accordingly, following a multiplicative decomposition for the deformation, and an additive decomposition for the stress, total stress can be expressed as (114–116)

$$\mathbf{S} = \mathbf{S}^{pas} + \mathbf{S}^{act}(\mathbf{F},\, \mathbf{F}^a). \quad 13.$$

The parallel spring gives rise to the passive response of the tissue (i.e., the response when no active contraction is present). Together, the series and contractile elements characterize the mechanics of muscle activation. The series element accounts for the additional elastic stiffness that arises when the cross-bridges are engaged (117). The contractile element generates the active force, representing the kinetics of cross-bridge sliding (Figure 2b).

4.4. Structural Modeling of Myocardium Involving Active Contraction

Overall, constitutive biomechanical modeling of contracting myocardium and the underlying mechanisms have been scarcely studied. Pioneering research pertaining to the biaxial characterization of myocardium during active contraction traces back to Lin & Yin (45). A significant finding of this study was the development of remarkably large forces in the cross-fiber direction (Figure 5a) that could not be explained solely by myofiber dispersion about the mean fiber direction. Surprisingly, very few similar studies were conducted thereafter. Recently, however, Krishnamurthy et al. (93) took an important step by developing a biophysical model that integrates cross-bridge mechanics with the passive behavior of myofibers to explain the interaction between the fiber and transverse directions in the active state. In summary, there remains a pressing need for 3D characterization of the mechanical behavior of contracting myocardium, as well as for the development of integrated structural models that can identify the role of myo- and collagen fibers and their interaction in the

contractile function of myocardium. Once implemented in an organ-level geometry, such models could provide new insights into the alterations of wall thickness during the cardiac cycle (21, 118).

5. FUTURE DIRECTIONS

5.1 Near-Term Landmarks

It should be clear from this review that comprehensive knowledge of the 3D mechanical behavior of myocardium is essential for understanding cardiac function in health and disease. Detailed tissue-level biomechanical models provide the mathematical framework for computational simulations that seek to link the structure and function of cardiac cells to the integrated behavior of the whole heart. While much progress has been made in such models, there remains a need for integrated approaches that enable (*a*) concise constitutive model forms to be developed on the basis of detailed tissue and cellular structural information, (*b*) identification of the optimal 3D tissue- and cellular-level experiments for model parameter identification, (*c*) experimental systems capable of conducting such 3D experiments, (*d*) comprehensive inverse finite element–based methods that fully integrate all experimental data to determine the best parameter estimates, and (*e*) greater use of Bayesian and related approaches to improve how we deal with the variation and uncertainty of the source data. Such integrated approaches will lay the groundwork for identifying, evaluating, and improving the optimal mathematical forms of the strain energy function when using a hyperelastic approach.

In the near term, a specific key issue to address is minimizing kinematic measures and material parameter covariances (119, 120). This review has demonstrated that much is to be gained from integrated studies on determination of an optimal form of a constitutive model (which entails minimal covariance between its constituent kinematic sets) in conjunction with optimizing the loading paths (which minimize the correlation between the material parameters). Concerning the latter, we have found that identifying optimal deformation modes (e.g., 82) is particularly critical for predicting tissue behavior under generalized deformation states not used in parameter estimation (13). More specifically, given that myocardial tissues undergo complex combinations of multiple deformation modes simultaneously in vivo, loading paths consisting of both simple shear and other 3D loading conditions are likely better choices for characterizing the myocardium response. However, it must be noted that the design of optimal loading paths is closely interlinked to the development of a constitutive model form, which is intrinsic to the nature of modeling non-linear materials. For planar tissues, we have recently developed such an integrated approach (121), and similar 3D works for myocardium remain to be explored. Overall, while we have conducted the first of such studies (13), this is only an initial step. For example, this comprehensive approach is indispensable for the case of treated diseased myocardium— such as hydrogel injection (10, 60, 122, 123)—where the local myocardium is subjected to more complex loading conditions. In addition, the development of appropriate instrumentation will be essential for the implementation of general loading paths and comprehensive exploration of optimal design of experiments.

After an appropriate constitutive law for myocardium is chosen, a remaining challenge is to reliably estimate the material constants such that they exhibit minimal dependence on the applied boundary conditions and experimental noise. This demand is especially prominent for in vivo applications, where the range of deformations can be dramatically limited compared with that experienced in vivo. Although many recent studies have explored the assimilation of different in vivo measurements to estimate these constants (124–128), another important aspect of such inverse problems that has not received adequate attention is the choice of optimization algorithm. Most studies so far have relied on either standard gradient-based optimization algorithms such as gradient descent and Levenberg–Marquardt, or gradient-free techniques such as genetic algorithms. However, the highly nonlinear nature of the forward problem and the presence of often strong statistical variation in the measurements demand the utilization of more robust algorithms that can (*a*) reduce the number of forward iterations and (*b*) directly account for the presence of the noise in the measurements. In this view, stochastic optimization methods such as Markov chain Monte Carlo (129) and Bayesian optimization algorithms (130, 131) that incorporate adjoint methods (132) offer scalability, higher speed, and enhanced robustness for identification of material constants.

Moreover, existing studies have modeled myocardium as an elastic material, whereas a few works have extended the invariant-based model to explore the viscoelastic behavior of myocardium (115, 133–135). Accounting for viscoelasticity is especially important for elastography applications to properly simulate the effects of acoustic wave dissipation. Finally, in our recent cardiac simulations, the effects of compressibility in myocardium in vivo (136) were profound. In particular, we found that the use of incompressibility can induce an up-to-twofold increase in the estimated contractile stresses. Such errors clearly indicate the need for greater fidelity in biomechanical modeling of the myocardium.

5.2. Greater Integration with the Underlying Structure and Insights into Growth and Remodeling

The morphology, structure, and functional mechanical properties of the myocardium are tightly interconnected. Clearly, existing structural approaches (87, 88) continue to rely on stochastic tissue-level structural data and approaches. Our ability to obtain cellular-level structural information (137) has greatly outpaced its use in biomechanical model development. Thus, a major challenge is to extend tissue-level stochastic approaches (87–89) to directly integrate detailed 3D structural information. Such approaches will enable a more direct connection between cellular and subcellular mechanisms and organ-level function.

These detailed structural approaches are especially necessary to describe growth and remodeling (G&R) (138). Roughly speaking, there are two types of mechanisms underlying G&R responses to environmental cues. The first type, associated with growth, induces changes in the mass and volume of fiber aggregates. The second type, associated with remodeling, alters the mechanical and structural properties of fiber ensembles. Despite significant progress in developing mathematical modeling that can reproduce the key manifestations of G&R events at both the tissue and organ levels, our understanding of how

the mechanisms at smaller scales, such as hypertrophy, atrophy, and fibrosis, can collectively lead to anatomical and functional changes in the heart remains very limited. To improve our understanding of these mechanisms and of their underlying mechanical stimulants, it is essential to conduct theory-driven experiments that can relate the contribution of each type of mechanism (taking place at the cellular level) to measurable changes in behavior at the tissue level (47). A crucial step in this approach is to develop new classes of mesoscale constitutive models that, on the one hand, can directly account for changes in the ratio and mechanical and structural properties of different tissue constituents and, on the other hand, remain tractable for implementation in organ-level simulations.

The tissue models discussed in this review are but one aspect of many that are required to fully describe the physiological function of the heart and its pathophysiology, as well as to develop novel therapies. Coupling not only to realistic geometries at all scales but also to electromechanical events and blood flow both within the ventricles and in the myocardium itself, detailed subcellular mechanisms (e.g., ion channel function) must ultimately be described within a single complete functional computational model. Until that time, as the great Y.C. Fung stated, "Let's enjoy the work" (139).

ACKNOWLEDGMENTS

LITERATURE CITED

1. Kehat I, Molkentin J. 2010 Molecular pathways underlying cardiac remodeling during pathophysiological stimulation. Circulation 122:2727–35 [PubMed: 21173361]

2. D'Ambra M, LaRaia P, Philbin D, Watkins W, Hilgenberg A, Buckley M. 1985 Prostaglandin E1. A new therapy for refractory right heart failure and pulmonary hypertension after mitral valve replacement. J. Thorac. Cardiovasc. Surg 89:567–72 [PubMed: 4039017]

3. Bogaard HJ, Abe K, Von Noordegraaf A, Voelkel NF. 2009 The right ventricle under pressure: cellular and molecular mechanisms of right-heart failure in pulmonary hypertension. Chest 135:794–804 [PubMed: 19265089]

4. Feldman A, McNamara D. 2000 Myocarditis. N. Engl. J. Med 343:1388–98 [PubMed: 11070105]

5. Jordan J, Todd R, Vasu S, Hundley W. 2018 Cardiovascular magnetic resonance in the oncology patient. JACC Cardiovasc. Imaging 11:1150–72 [PubMed: 30092971]

6. Sukhovershin R, Cooke J. 2016 How may proton pump inhibitors impair cardiovascular health? Am. J. Cardiovasc. Drugs 16:153–61 [PubMed: 26817947]

7. Rosenzweig A 2012 Cardiac regeneration. Science 338:1549–50 [PubMed: 23258880]

8. Nadruz W 2015 Myocardial remodeling in hypertension. J. Hum. Hypertens 29:1–6 [PubMed: 24804791]

9. Holmes J, Borg T, Covell J. 2005 Structure and mechanics of healing myocardial infarcts. Annu. Rev. Biomed. Eng 7:223–53 [PubMed: 16004571]

10. Wall S, Walker J, Healy K, Ratcliffe M, Guccione J. 2006 Theoretical impact of the injection of material into the myocardium: a finite element model simulation. Circulation 114:2627–35 [PubMed: 17130342]

11. Humphrey J 2013 Cardiovascular Solid Mechanics: Cells, Tissues, and Organs Berlin: Springer Sci. Bus. Media

12. Soares J, Feaver K, Zhang W, Kamensky D, Aggarwal A, Sacks M. 2016 Biomechanical behavior of bioprosthetic heart valve heterograft tissues: characterization, simulation, and performance. Cardiovasc. Eng. Technol 7:309–51 [PubMed: 27507280]

13. Avazmohammadi R, Li D, Leahy T, Shih E, Soares J, et al. 2018 An integrated inverse model-experimental approach to determine soft tissue three-dimensional constitutive parameters: application to post-infarcted myocardium. Biomech. Model. Mechanobiol 17:31–53 [PubMed: 28861630]

14. Bers D 2002 Cardiac excitation–contraction coupling. Nature 415:198–205 [PubMed: 11805843]

15. de Tombe P 2003 Cardiac myofilaments: mechanics and regulation. J. Biomech 36:721–30 [PubMed: 12695002]

16. Hunter P, Smaill B. 1988 The analysis of cardiac function: a continuum approach. Prog. Biophys. Mol. Biol 52:101–64 [PubMed: 3076684]

17. ter Keurs H 1995 Sarcomere function and crossbridge cycling. In Molecular and Subcellular Cardiology, ed. Sideman S, Beyar R, pp. 125–35. Berlin: Springer

18. Sengupta P, Krishnamoorthy V, Korinek J, Narula J, Vannan M, et al. 2007 Left ventricular form and function revisited: applied translational science to cardiovascular ultrasound imaging. J. Am. Soc. Echocardiogr 20:539–51 [PubMed: 17485001]

19. Clayton R, Bernus O, Cherry E, Dierckx H, Fenton F, et al. 2011 Models of cardiac tissue electrophysiology: progress, challenges and open questions. Prog. Biophys. Mol. Biol 104:22–48 [PubMed: 20553746]

20. Streeter D Jr., Spotnitz H, Patel D, Ross J Jr., Sonnenblick E. 1969 Fiber orientation in the canine left ventricle during diastole and systole. Circ. Res 24:339–47 [PubMed: 5766515]

21. Lunkenheimer P, Redmann K, Kling N, Jiang X, Rothaus K, et al. 2006 Three-dimensional architecture of the left ventricular myocardium. Anat. Rec. A 288:565–78

22. Curtis M, Russell B. 2011 Micromechanical regulation in cardiac myocytes and fibroblasts: implications for tissue remodeling. Pflüg. Arch. Eur. J. Physiol 462:105–17

23. Kelly DE, Wood RL, Enders AC. 1984 Textbook of Microscopic Anatomy 18th ed. Baltimore: Williams & Wilkins http://www.columbia.edu/itc/hs/medical/sbpm_histology_old/lab/micro_popup21.html

24. Rausch M, Dam A, Göktepe S, Abilez OJ, Kuhl E. 2011 Computational modeling of growth: systemic and pulmonary hypertension in the heart. Biomech. Model. Mechanobiol 10:799–811 [PubMed: 21188611]

25. LeGrice I, Smaill B, Chai L, Edgar S, Gavin J, Hunter P. 1995 Laminar structure of the heart: ventricular myocyte arrangement and connective tissue architecture in the dog. Am. J. Physiol. Heart Circ. Physiol 269:H571–82

26. Intrigila B, Melatti I, Tofani A, Macchiarelli G. 2007 Computational models of myocardial endomysial collagen arrangement. Comput. Methods Programs Biomed 86:232–44 [PubMed: 17451838]

27. Anderson R, Smerup M, Sanchez-Quintana D, Loukas M, Lunkenheimer P. 2009 The three-dimensional arrangement of the myocytes in the ventricular walls. Clin. Anat 22:64–76 [PubMed: 18567009]

28. Peterson DR, Bronzino JD. 2007 Biomechanics: Principles and Applications 2nd ed. Boca Raton, FL: CRC

29. Macchiarelli G, Ohtani O, Nottola S, Stallone T, Camboni A, et al. 2002 A micro-anatomical model of the distribution of myocardial endomysial collagen. Histol. Histopathol 17:699–706 [PubMed: 12168777]

30. Fomovsky G, Thomopoulos S, Holmes J. 2010 Contribution of extracellular matrix to the mechanical properties of the heart. J. Mol. Cell. Cardiol 48:490–96 [PubMed: 19686759]

31. Leonard B, Smaill B, LeGrice I. 2012 Structural remodeling and mechanical function in heart failure. Microsc. Microanal 18:50–67 [PubMed: 22258722]

32. Robinson T, Factor S, Sonnenblick E. 1986 The heart as a suction pump. Sci. Am 254:84–91 [PubMed: 3704622]

33. Rohmer D, Sitek A, Gullberg G. 2007 Reconstruction and visualization of fiber and laminar structure in the normal human heart from ex vivo diffusion tensor magnetic resonance imaging (DTMRI) data. Investig. Radiol 42:777–89 [PubMed: 18030201]

34. Robinson T, Cohen-Gould L, Factor S. 1983 Skeletal framework of mammalian heart muscle. Arrangement of inter- and pericellular connective tissue structures. Lab. Investig 49:482–98 [PubMed: 6684712]

35. Caulfield J, Borg T. 1979 The collagen network of the heart. Lab. Investig 40:364–72 [PubMed: 423529]

36. Borg T, Caulfield J. 1981 The collagen matrix of the heart. Fed. Proc 40:2037–41 [PubMed: 7227559]

37. Borg T, Johnson L, Lill P. 1983 Specific attachment of collagen to cardiac myocytes: in vivo and in vitro. Dev. Biol 97:417–23 [PubMed: 6852372]

38. Torrent-Guasp F, Buckberg GD, Clemente C, Cox JL, Coghlan HC, Gharib M. 2001 The structure and function of the helical heart and its buttress wrapping. I. The normal macroscopic structure of the heart. Semin. Thorac. Cardiovasc. Surg 13:201–19 [PubMed: 11568867]

39. Buckberg G 2002 Basic science review: the helix and the heart. J. Thorac. Cardiovasc. Surg 124:863–83 [PubMed: 12407367]

40. Burton R, Plank G, Schneider J, Grau V, Ahammer H, et al. 2006 Three-dimensional models of individual cardiac histoanatomy: tools and challenges. Ann. N. Y. Acad. Sci 1080:301–19 [PubMed: 17132791]

41. Nash M, Hunter P. 2000 Computational mechanics of the heart. J. Elast 61:113–41

42. Nielles-Vallespin S, Mekkaoui C, Gatehouse P, Reese TG, Keegan J, et al. 2013 In vivo diffusion tensor MRI of the human heart: reproducibility of breath-hold and navigator-based approaches. Magn. Reson. Med 70:454–65 [PubMed: 23001828]

43. Helm P, Tseng H, Younes L, McVeigh E, Winslow R. 2005 Ex vivo 3D diffusion tensor imaging and quantification of cardiac laminar structure. Magn. Reson. Med 54:850–59 [PubMed: 16149057]

44. Jang S, Vanderpool R, Avazmohammedi R, Lapshin E, Bachman TN, et al. 2017 Biomechanical and hemodynamic measures of right ventricular diastolic function: translating tissue biomechanics to clinical relevance. J. Am. Heart Assoc 6:e006084 [PubMed: 28899895]

45. Lin D, Yin F. 1998 A multiaxial constitutive law for mammalian left ventricular myocardium in steady-state barium contracture or tetanus. J. Biomech. Eng 120:504–17 [PubMed: 10412422]

46. Parker K, Ingber D. 2007 Extracellular matrix, mechanotransduction and structural hierarchies in heart tissue engineering. Philos. Trans. R. Soc. B 362:1267–79

47. Avazmohammadi R, Hill M, Simon M, Sacks M. 2017 Transmural remodeling of right ventricular myocardium in response to pulmonary arterial hypertension. APL Bioeng 1:016105 [PubMed: 30417163]

48. Couade M, Pernot M, Messas E, Bel A, Ba M, et al. 2011 In vivo quantitative mapping of myocardial stiffening and transmural anisotropy during the cardiac cycle. IEEE Trans. Med. Imaging 30:295–305 [PubMed: 20851788]

49. Arts T, Costa K, Covell J, McCulloch A. 2001 Relating myocardial laminar architecture to shear strain and muscle fiber orientation. Am. J. Physiol. Heart Circ. Physiol 280:H2222–29 [PubMed: 11299225]

50. Sandler H, Dodge H. 1963 Left ventricular tension and stress in man. Circ. Res 13:91–104 [PubMed: 14047642]

51. Falsetti H, Mates R, Grant C, Greene D, Bunnell I. 1970 Left ventricular wall stress calculated from one-plane cineangiography: an approach to force–velocity analysis in man. Circ. Res 26:71–83 [PubMed: 5410094]

52. Gaasch W, Levine H, Quinones M, Alexander J. 1976 Left ventricular compliance: mechanisms and clinical implications. Am. J. Cardiol 38:645–53 [PubMed: 136186]

53. Yin F 1981 Ventricular wall stress. Circ. Res 49:829–42 [PubMed: 7023741]

54. Fifer M, Grossman W. 2013 Measurement of ventricular volumes, ejection fraction, mass, wall stress, and regional wall motion. In Grossman & Baim's Cardiac Catheterization, Angiography, and Intervention, ed. Moscucci M, pp. 310–12. Baltimore: Lippincott, Williams & Wilkins 8th ed.

55. Basford J 2002 The Law of Laplace and its relevance to contemporary medicine and rehabilitation. Arch. Phys. Med. Rehabil 83:1165–70 [PubMed: 12161841]

56. Genet M, Lee L, Nguyen R, Haraldsson H, Acevedo-Bolton G, et al. 2014 Distribution of normal human left ventricular myofiber stress at end diastole and end systole: a target for in silico design of heart failure treatments. J. Appl. Physiol 117:142–52 [PubMed: 24876359]

57. Lee L, Ge L, Zhang Z, Pease M, Nikolic S, et al. 2014 Patient-specific finite element modeling of the Cardiokinetix Parachute® device: effects on left ventricular wall stress and function. Med. Biol. Eng 52:557–66

58. Bosi G, Capelli C, Khambadkone S, Taylor A, Schievano S. 2015 Patient-specific finite element models to support clinical decisions: a lesson learnt from a case study of percutaneous pulmonary valve implantation. Catheter. Cardiovasc. Interv 86:1120–30 [PubMed: 25855063]

59. Wenk J, Wall S, Peterson R, Helgerson S, Sabbah H, et al. 2009 A method for automatically optimizing medical devices for treating heart failure: designing polymeric injection patterns. J. Biomech. Eng 131:121011 [PubMed: 20524734]

60. Lee L, Wall S, Genet M, Hinson A, Guccione J. 2014 Bioinjection treatment: effects of post-injection residual stress on left ventricular wall stress. J. Biomech 47:3115–19 [PubMed: 25065728]

61. Fung Y 2013 Biomechanics: Mechanical Properties of Living Tissues Berlin: Springer Sci. Bus. Media

62. Chadwick P 2012 Continuum Mechanics: Concise Theory and Problems North Chelmsford, MA: Courier

63. Gurtin ME. 1982 An Introduction to Continuum Mechanics. Math. Sci. Eng vol. 158 San Diego: Academic

64. Fuchs R, Brinker J, Maughan W, Weisfeldt M, Yin F. 1981 Coronary flow limitation during the development of ischemia: effect of atrial pacing in patients with left anterior descending coronary artery disease. Am. J. Cardiol 48:1029–36 [PubMed: 7304454]

65. Yeoh O 1993 Some forms of the strain energy function for rubber. Rubber Chem. Technol 66:754–71

66. Guccione J, McCulloch A, Waldman L. 1991 Passive material properties of intact ventricular myocardium determined from a cylindrical model. J. Biomech. Eng 113:42–55 [PubMed: 2020175]

67. Humphrey J, Yin F. 1987 On constitutive relations and finite deformations of passive cardiac tissue. I. A pseudostrain–energy function. J. Biomech. Eng 109:298–304 [PubMed: 3695429]

68. Humphrey J, Strumpf R, Yin F. 1990 Determination of a constitutive relation for passive myocardium. II. Parameter estimation. J. Biomech. Eng 112:340–46 [PubMed: 2214718]

69. Kerckhoffs R, Bovendeerd P, Kotte J, Prinzen F, Smits K, Arts T. 2003 Homogeneity of cardiac contraction despite physiological asynchrony of depolarization: a model study. Ann. Biomed. Eng 31:536–47 [PubMed: 12757198]

70. Holzapfel G, Ogden R. 2009 Constitutive modelling of passive myocardium: a structurally based framework for material characterization. Philos. Trans. R. Soc. A 367:3445–75

71. Schmid H, Wang Y, Ashton J, Ehret A, Krittian S, et al. 2009 Myocardial material parameter estimation: a comparison of invariant based orthotropic constitutive equations. Comput. Methods Biomech. Biomed. Eng 12:283–95

72. Yin F, Strumpf R, Chew P, Zeger S. 1987 Quantification of the mechanical properties of noncontracting canine myocardium under simultaneous biaxial loading. J. Biomech 20:577–89 [PubMed: 3611134]

73. Hill M, Simon M, Valdez-Jasso D, Zhang W, Champion H, Sacks M. 2014 Structural and mechanical adaptations of right ventricle free wall myocardium to pressure overload. Ann. Biomed. Eng 42:2451–65 [PubMed: 25164124]

74. Hunter P, Nash M, Sands G. 1997 Computational biology of the heart. In Computational Electromechanics of the Heart, ed. Panfilov AV, Holden AV, pp. 345–407. West Sussex, UK: Wiley

75. Costa K, Holmes J, McCulloch A. 2001 Modelling cardiac mechanical properties in three dimensions. Philos. Trans. R. Soc. A 359:1233–50

76. Schmid H, Nash M, Young A, Hunter P. 2006 Myocardial material parameter estimation: a comparative study for simple shear. J. Biomech. Eng 128:742–50 [PubMed: 16995761]

77. Murphy J 2013 Transversely isotropic biological, soft tissue must be modelled using both anisotropic invariants. Eur. J. Mech. A 42:90–96

78. Humphrey J, Strumpf R, Yin F. 1990 Determination of a constitutive relation for passive myocardium. I. A new functional form. J. Biomech. Eng 112:333–39 [PubMed: 2214717]

79. Dokos S, Smaill B, Young A, LeGrice I. 2002 Shear properties of passive ventricular myocardium. Am. J. Physiol. Heart Circ. Physiol 283:H2650–59 [PubMed: 12427603]

80. Humphrey J, Yin F. 1989 Biomechanical experiments on excised myocardium: theoretical considerations. J. Biomech 22:377–83 [PubMed: 2745472]

81. Merodio J, Ogden RW. 2006 The influence of the invariant I8 on the stress–deformation and ellipticity characteristics of doubly fiber-reinforced non-linearly elastic solids. Int. J. Non-Linear Mech 41:556–63

82. Lanir Y, Lichtenstein O, Imanuel O. 1996 Optimal design of biaxial tests for structural material characterization of flat tissues. J. Biomech. Eng 118:41–47 [PubMed: 8833073]

83. Sacks M 2000 Biaxial mechanical evaluation of planar biological materials. J. Elast 61:199

84. Choi H, Vito R. 1990 Two-dimensional stress–strain relationship for canine pericardium. J. Biomech. Eng 112:153–59 [PubMed: 2345445]

85. Costa K, Takayama Y, McCulloch A, Covell J. 1999 Laminar fiber architecture and three-dimensional systolic mechanics in canine ventricular myocardium. Am. J. Physiol. Heart Circ. Physiol 276:H595–607

86. Smaill B, Hunter P. 1991 Structure and function of the diastolic heart: material properties of passive myocardium. In Theory of Heart, ed. Glass L, Hunter P, McCulloch A, pp. 1–29. New York: Springer

87. Horowitz A, Lanir Y, Yin F, Perl M, Sheinman I, Strumpf R. 1988 Structural three-dimensional constitutive law for the passive myocardium. J. Biomech. Eng 110:200–7 [PubMed: 3172739]

88. Avazmohammadi R, Hill M, Simon MA, Zhang W, Sacks MS. 2017 A novel constitutive model for passive right ventricular myocardium: evidence for myofiber–collagen fiber mechanical coupling. Biomech. Model. Mechanobiol 16:561–81 [PubMed: 27696332]

89. Lanir Y 1983 Constitutive equations for the lung tissue. J. Biomech. Eng 105:374–80 [PubMed: 6645447]

90. Sacks M, Chuong C. 1993 A constitutive relation for passive right-ventricular free wall myocardium. J. Biomech 26:1341–45 [PubMed: 8262995]

91. Lee L, Wenk J, Klepach D, Kassab G, Guccione J. 2016 Structural-based models of ventricular myocardium. In Structure-Based Mechanics of Tissues and Organs, ed. Kassab G, Sacks MS, pp. 249–63. Berlin: Springer

92. Eriksson T, Prassl A, Plank G, Holzapfel G. 2013 Influence of myocardial fiber/sheet orientations on left ventricular mechanical contraction. Math. Mech. Solids 18:592–606

93. Krishnamurthy A, Coppola B, Tangney J, Kerckhoffs R, Omens J, McCulloch A. 2016 A microstructurally based multi-scale constitutive model of active myocardial mechanics. In Structure-Based Mechanics of Tissues and Organs, ed. Kassab G, Sacks MS, pp. 439–60. Berlin: Springer

94. Ostoja-Starzewski M 2007 Microstructural Randomness and Scaling in Mechanics of Materials Boca Raton, FL: Chapman & Hall/CRC

95. Sommer G, Schriefl A, Andrä M, Sacherer M, Viertler C, et al. 2015 Biomechanical properties and microstructure of human ventricular myocardium. Acta Biomater 24:172–92 [PubMed: 26141152]

96. Palit A, Bhudia S, Arvanitis T, Turley G, Williams M. 2015 Computational modelling of left-ventricular diastolic mechanics: effect of fibre orientation and right-ventricle topology. J. Biomech 48:604–12 [PubMed: 25596634]

97. Nikou A, Gorman R, Wenk J. 2016 Sensitivity of left ventricular mechanics to myofiber architecture: a finite element study. Proc. Inst. Mech. Eng. H 230:594–98 [PubMed: 26975892]

98. Rodríguez-Cantano R, Sundnes J, Rognes M. 2018 Uncertainty in cardiac myofiber orientation and stiffnesses dominate the variability of left ventricle deformation response. arXiv:1801.02989 [physics.comp-ph]

99. Pathmanathan P, Chapman S, Gavaghan D, Whiteley J. 2010 Cardiac electromechanics: the effect of contraction model on the mathematical problem and accuracy of the numerical scheme. Q. J. Mech. Appl. Math 63:375–99

100. Trayanova N, Rice J. 2011 Cardiac electromechanical models: from cell to organ. Front. Physiol 2:43 [PubMed: 21886622]

101. Hunter P, McCulloch A, Ter Keurs H. 1998 Modelling the mechanical properties of cardiac muscle. Prog. Biophys. Mol. Biol 69:289–331 [PubMed: 9785944]

102. Guccione J, McCulloch A. 1993 Mechanics of active contraction in cardiac muscle. Part I. Constitutive relations for fiber stress that describe deactivation. J. Biomech. Eng 115:72–81 [PubMed: 8445901]

103. Guccione J, McCulloch A. 1993 Mechanics of active contraction in cardiac muscle. Part II. Cylindrical models of the systolic left ventricle. J. Biomech. Eng 115:82–90 [PubMed: 8445902]

104. Wang Y 2012 Modelling in vivo cardiac mechanics using MRI and FEM PhD thesis, Univ. Auckland, Auckland, N. Z.

105. Costabal F, Concha F, Hurtado D, Kuhl E. 2017 The importance of mechano-electrical feedback and inertia in cardiac electromechanics. Comput. Methods Appl. Mech. Eng 320:352–68 [PubMed: 29056782]

106. Nardinocchi P, Teresi L. 2007 On the active response of soft living tissues. J. Elast 88:27–39

107. Cherubini C, Filippi S, Nardinocchi P, Teresi L. 2008 An electromechanical model of cardiac tissue: constitutive issues and electrophysiological effects. Prog. Biophys. Mol. Biol 97:562–73 [PubMed: 18353430]

108. Ambrosi D, Arioli G, Nobile F, Quarteroni A. 2011 Electromechanical coupling in cardiac dynamics: the active strain approach. SIAM J. Appl. Math 71:605–21

109. Nobile F, Quarteroni A, Ruiz-Baier R. 2012 An active strain electromechanical model for cardiac tissue. Int. J. Numer. Methods Biomed. Eng 28:52–71

110. Ruiz-Baier R, Gizzi A, Rossi S, Cherubini C, Laadhari A, et al. 2013 Mathematical modelling of active contraction in isolated cardiomyocytes. Math. Med. Biol 31:259–83 [PubMed: 23760444]

111. Quarteroni A, Lassila T, Rossi S, Ruiz-Baier R. 2017 Integrated heart coupling multiscale and multi-physics models for the simulation of the cardiac function. Comput. Methods Appl. Mech. Eng 314:345–407

112. Rossi S, Lassila T, Ruiz-Baier R, Sequeira A, Quarteroni A. 2014 Thermodynamically consistent orthotropic activation model capturing ventricular systolic wall thickening in cardiac electromechanics. Eur. J. Mech. A 48:129–42

113. Hill A 1938 The heat of shortening and the dynamic constants of muscle. Proc. R. Soc. Lond. B 126:136–95

114. Göktepe S, Menzel A, Kuhl E. 2014 The generalized Hill model: a kinematic approach towards active muscle contraction. J. Mech. Phys. Solids 72:20–39 [PubMed: 25221354]

115. Ponnaluri A, Perotti L, Ennis D, Klug W. 2017 A viscoactive constitutive modeling framework with variational updates for the myocardium. Comput. Methods Appl. Mech. Eng 314:85–101 [PubMed: 28579649]

116. Cansız B, Dal H, Kaliske M. 2017 Computational cardiology: a modified Hill model to describe the electro-visco-elasticity of the myocardium. Comput. Methods Appl. Mech. Eng 315:434–66

117. Ponnaluri AVS. 2018 Cardiac electromechanics modeling and validation PhD thesis, Univ. Calif., Los Angeles

118. Sallin E 1969 Fiber orientation and ejection fraction in the human left ventricle. Biophys. J 9:954–64 [PubMed: 5791550]

119. Criscione J, McCulloch A, Hunter W. 2002 Constitutive framework optimized for myocardium and other high-strain, laminar materials with one fiber family. J. Mech. Phys. Solids 50:1681–702

120. Criscione J 2004 Rivlin's representation formula is ill-conceived for the determination of response functions via biaxial testing. In The Rational Spirit in Modern Continuum Mechanics, ed. Man C-S, Fosdick RL, pp. 197–215. Berlin: Springer

121. Zhang W, Zakerzadeh R, Zhang W, Sacks M. 2019 A material modeling approach for the effective response of planar soft tissues for efficient computational simulations. J. Mech. Behav. Biomed. Mater 89:168–98 [PubMed: 30286376]

122. Dorsey S, McGarvey J, Wang H, Nikou A, Arama L, et al. 2015 MRI evaluation of injectable hyaluronic acid–based hydrogel therapy to limit ventricular remodeling after myocardial infarction. Biomaterials 69:65–75 [PubMed: 26280951]

123. Wang H, Rodell CB, Zhang X, Dusaj N, Gorman J, et al. 2018 Effects of hydrogel injection on borderzone contractility post-myocardial infarction. Biomech. Model. Mechanobiol 17:1533–42 [PubMed: 29855734]

124. Xi J, Lamata P, Shi W, Niederer S, Land S, et al. 2011 An automatic data assimilation framework for patient-specific myocardial mechanical parameter estimation. In Proceedings of the 6th International Conference on Functional Imaging and Modeling of the Heart, ed. Metaxas DN, Axel L, pp. 392–400. Berlin: Springer

125. Asner L, Hadjicharalambous M, Chabiniok R, Peresutti D, Sammut E, et al. 2016 Estimation of passive and active properties in the human heart using 3D tagged MRI. Biomech. Model. Mechanobiol 15:1121–39 [PubMed: 26611908]

126. Nasopoulou A, Shetty A, Lee J, Nordsletten D, Rinaldi C, et al. 2017 Improved identifiability of myocardial material parameters by an energy-based cost function. Biomech. Model. Mechanobiol 16:971–88 [PubMed: 28188386]

127. Perotti L, Ponnaluri A, Krishnamoorthi S, Balzani D, Ennis D, Klug W. 2017 Method for the unique identification of hyperelastic material properties using full-field measures. Application to the passive myocardium material response. Int. J. Numer. Methods Biomed. Eng 33:e2866

128. Palit A, Bhudia S, Arvanitis T, Turley G, Williams M. 2018 In vivo estimation of passive biomechanical properties of human myocardium. Med. Biol. Eng 56:1615–31

129. Johnstone R, Chang E, Bardenet R, De Boer T, Gavaghan D, et al. 2016 Uncertainty and variability in models of the cardiac action potential: Can we build trustworthy models? J. Mol. Cell. Cardiol 96:49–62 [PubMed: 26611884]

130. Perdikaris P, Karniadakis G. 2016 Model inversion via multi-fidelity Bayesian optimization: a new paradigm for parameter estimation in haemodynamics, and beyond. J. R. Soc. Interface 13:20151107 [PubMed: 27194481]

131. Giffard-Roisin S, Delingette H, Jackson T, Fovargue L, Lee J, et al. 2017 Sparse Bayesian non-linear regression for multiple onsets estimation in non-invasive cardiac electrophysiology. In Proceedings of the 9th International Conference on Functional Imaging and Modeling of the Heart, ed. Pop M, Wright GA, pp. 230–38. Berlin: Springer

132. Balaban G, Alnæs M, Sundnes J, Rognes M. 2016 Adjoint multi-start-based estimation of cardiac hyperelastic material parameters using shear data. Biomech. Model. Mechanobiol 15:1509–21 [PubMed: 27008196]

133. Cansız F, Dal H, Kaliske M. 2015 An orthotropic viscoelastic material model for passive myocardium: theory and algorithmic treatment. Comput. Methods Biomech. Biomed. Eng 18:1160–72

134. Cansız B, Dal H, Kaliske M. 2015 Fully coupled cardiac electromechanics with orthotropic viscoelastic effects. Proc. IUTAM 12:124–33

135. Gültekin O, Sommer G, Holzapfel G. 2016 An orthotropic viscoelastic model for the passive myocardium: continuum basis and numerical treatment. Comput. Methods Biomech. Biomed. Eng 19:1647–64

136. Soares J, Li D, Lai E, Gorman J, Gorman R, Sacks M. 2017 Modeling of myocardium compressibility and its impact in computational simulations of the healthy and infarcted heart. In Proceedings of the 9th International Conference on Functional Imaging and Modeling of the Heart, ed. Pop M, Wright GA, pp. 493–501. Berlin: Springer

137. Lasher R, Hitchcock R, Sachse F. 2009 Towards modeling of cardiac micro-structure with catheter-based confocal microscopy: a novel approach for dye delivery and tissue characterization. IEEE Trans. Med. Imaging 28:1156–64 [PubMed: 19336297]

138. Wang V, Hussan J, Yousefi H, Bradley C, Hunter P, Nash M. 2017 Modelling cardiac tissue growth and remodelling. J. Elast 129:283–305

139. Fung Y 2002 Celebrating the inauguration of the journal: Biomechanics and Modeling in Mechanobiology. Biomech. Model. Mechanobiol 1:3–4
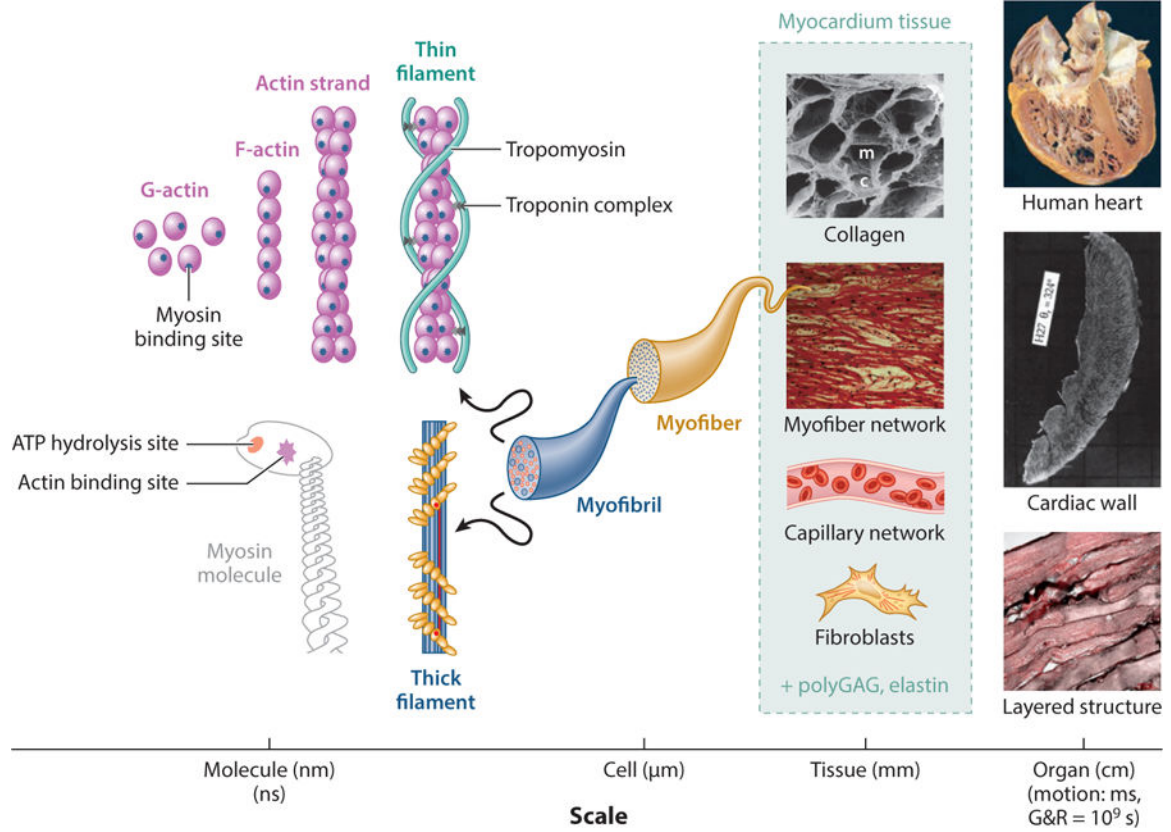
Figure 1.
Structural hierarchy involved in myocardium tissue. Understanding of the tissue behavior at the mesoscale can better inform both the organ-scale behavior and the cellular and subcellular behavior. Abbreviations: ATP, adenosine triphosphate; c, capillary lacunae; G&R, growth and remodeling; m, myofiber lacunae; polyGAG, polyglycosaminoglycan. Images of the human heart, cardiac wall, collagen, and myofiber network are from References 24, 25, 26, and 27, respectively. The image of the layered structure is an unpublished image taken at the Willerson Center at the University of Texas, Austin.
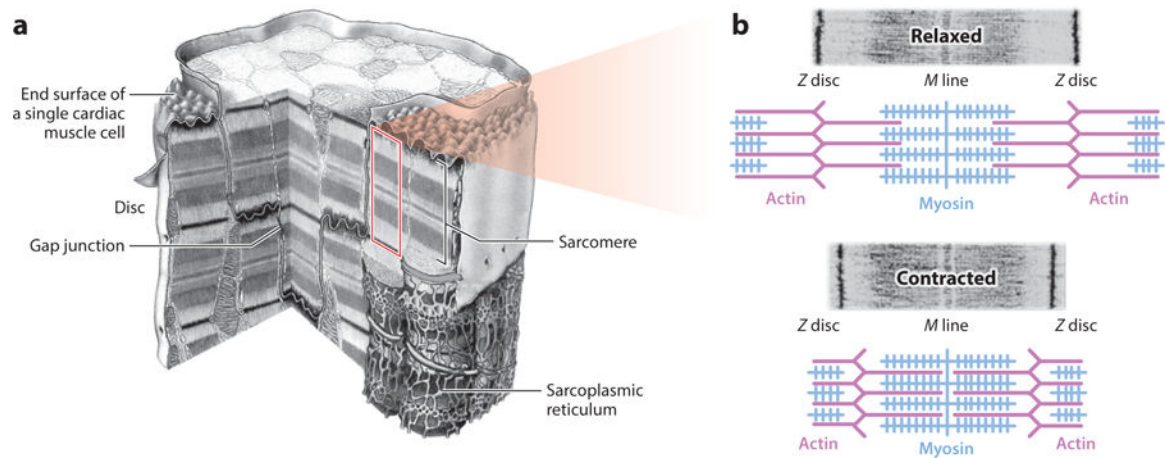
Figure 2.
(*a*) Cutaway view of a cardiac myocyte, including several sarcomere units. (*b*) Machinery schematic for active muscle contraction via cross-bridge cycling. The central blue rods represent several myosin molecules (thick filament) with the actin binding site projecting out, surrounded by thin purple filaments. Titin proteins support the thick filament. Panel *a* adapted from Reference 23. Panel *b* adapted with permission from Pearson Education, Inc. Copyright 2004.
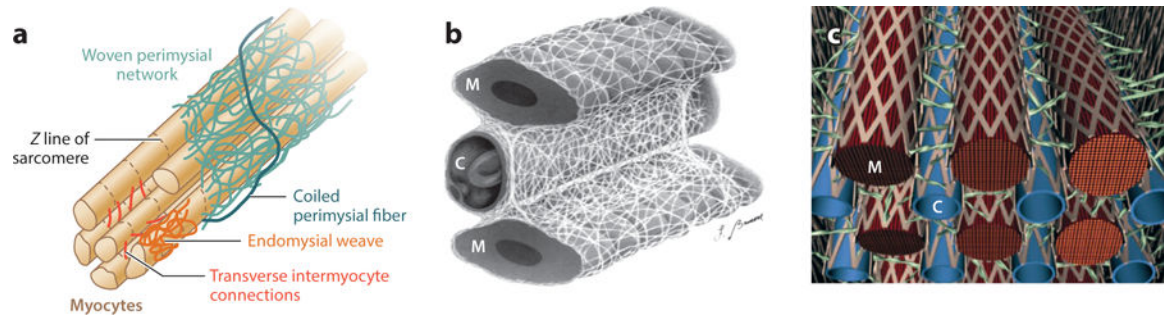
Figure 3.

Different representations of the microstructural details of the collagen fiber arrangement in myocardium. (*a*) Arrangement of endomysial and perimysial collagen fibers with respect to myofibers. (*b*) Sheath-like arrangement of fine endomysial collagen fiber network. (*c*) Strut and weave representations of collagen fibers around myofibers (M) and capillary vessels (C). Panel *a* adapted from Reference 28. Panel *b* reprinted from Reference 29.
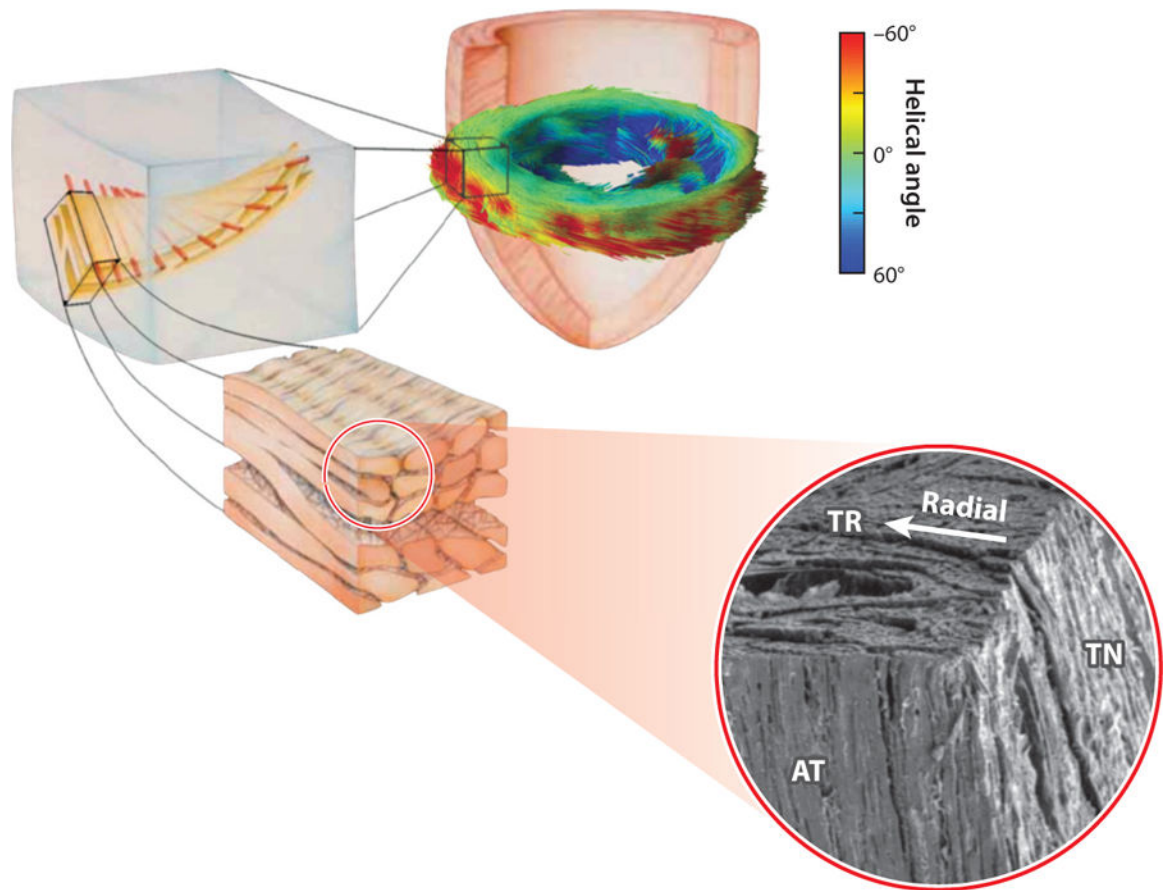
Figure 4.
Schematic of cardiac microstructure showing transmural fiber orientation and branching
sheet structures. Abbreviations: TR, transverse; AT, axial-transmural; TN, tangential planes.
Combined figure adapted from References 25, 41, and 42.
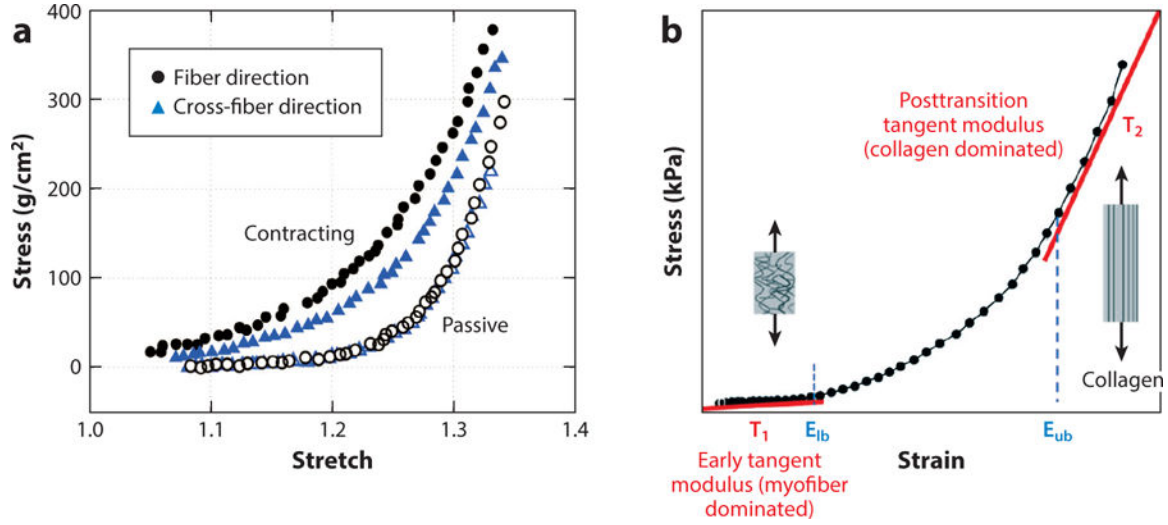
Figure 5.
(*a*) Active contraction in fiber and cross-fiber directions observed by Lin & Yin (45) (using barium contracture in rabbit left ventricular tissue). (*b*) Stress–strain curve showing three distinct stiffness regions—myofiber dominated, transitioning, and collagen dominated—in the passive biomechanical response of myocardium. E_{lb} and E_{ub} represent the lower and upper bound strains of collagen recruitment, respectively. Panel *b* adapted from Reference 44.
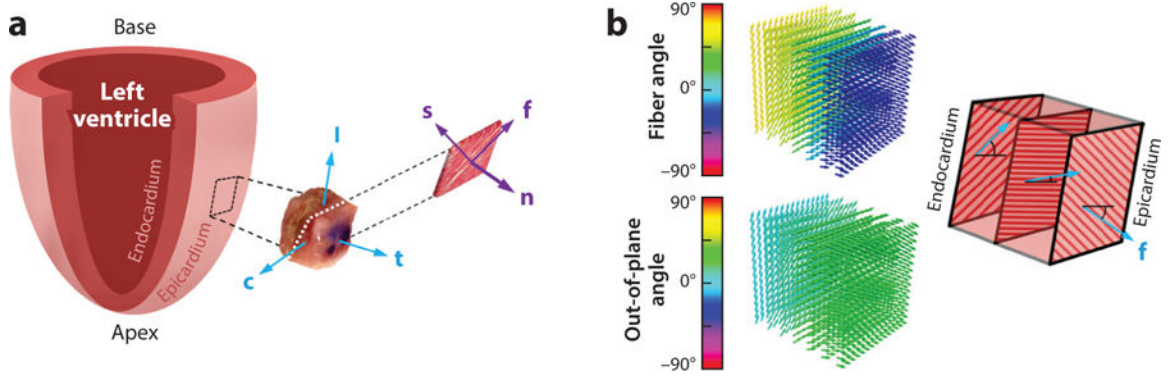
Figure 6.

(a) Schematic representation of the fiber–sheet–normal microstructure. The mean myofiber direction is denoted by the vector **f**, the direction transverse to the fiber axis within the layers is denoted by **s**, and the direction normal to the layers is denoted by **n**. (*b*) Model of the heart wall as a layered structure, with each layer exhibiting transverse isotropy. Other vectors: **c**, circumferential direction; **l**, longitudinal direction; **t**, transmural direction. Panel *a* inspired by Reference 79. Panel *b* inspired by Reference 80.
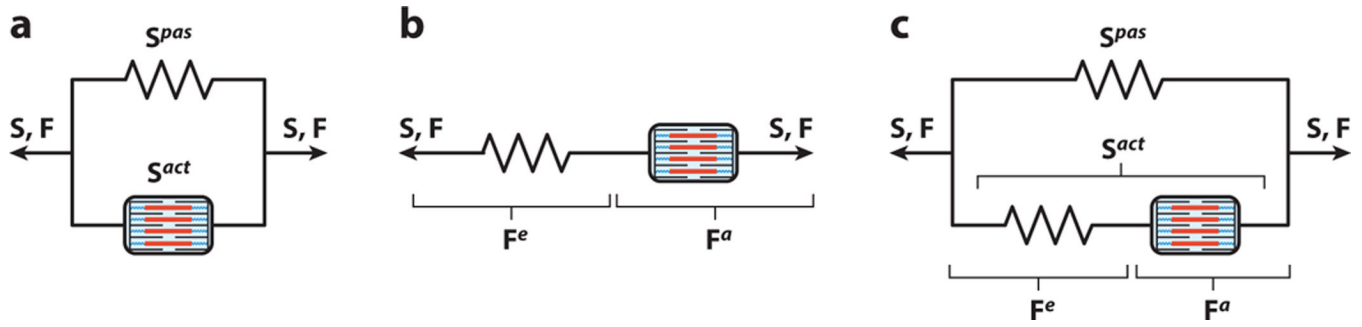
Figure 7.
Schematic representations of active contraction model. (*a*) Active stress model consisting of a contractile element in parallel with the passive spring element. (*b*) The active strain model consisting of a passive spring element in series with a contractile element. (*c*) Hill's three-element model consisting of two spring elements in parallel and in series with a contractile element. Abbreviations: *a* and *act*, active; *e*, elastic; *pas*, passive; **S** and **F**, total stress and deformation gradient tensors, respectively.

Table 1

Summary of phenomenological constitutive models for passive behavior of myocardium[a]

Invariant-based models: $W = \Psi(I_i)$		
Isotropic $W = \Psi(I_1, I_2)$	Fuchs et al. (64) $\Psi = A(I_1 - 3) + B(I_2 - 3)$	Guccione et al. (66) $\Psi = A\left[e^{B(I_1 - 3)} - 1\right]$
Transversely isotropic $W = \Psi(I_1, I_2, I_4)$	Humphrey & Yin (67) $\Psi = A\left[e^{B(I_1 - 3)} - 1\right] + C[e^{D(\sqrt{I_4} - 1)^2} - 1]$	Humphrey et al. (68) $\Psi = \sum_{i=1}^{2} A_i (I_1 - 3)^i + \sum_{i=1}^{2} B_i (\sqrt{I_4} - 1)^{i+1} + C(I_1 - 3)(\sqrt{I_4} - 1)$
	Lin & Yin (45) $W = A(e^Q - 1),$ $Q = B_1(I_1 - 3)^2 + B_2(I_1 - 3)(I_4 - 1) + B_3(I_4 - 1)^2$	
	Kerckhoffs et al. (69) $\Psi = A\{e^{[B I_1^2 + C I_2 - (3B+C)(2I_1 - 3)]} - 1\} + D[e^{E(I_4 - 1)^2} - 1]$	
Orthotropic $W = \Psi(I_1, I_2, I_4, I_6, I_8)$	Holzapfel & Ogden (70) $\Psi = A\left[e^{B(I_1 - 3)} - 1\right] + C[e^{D(I_4 - 1)^2} - 1] + E[e^{F(I_6 - 1)^2} - 1] + G[e^{H I_8^2} - 1]$	
	Schmid et al. (71) $\Psi = A[e^{B(I_1 - 3)^2} - 1] + C[e^{D(I_2 - 3)^2} - 1] + \sum_{i}^{f,s,n} E_i[e^{F_i(I_i - 1)^2} - 1]$	
Strain component–based models: $W = \Psi(E_{ij})$		
Transversely isotropic	Yin et al. (72) $\Psi = A[e^{B_1 E_{11}^n + B_2 E_{22}^n} - 1]$	Guccione et al. (66) $\Psi = A\left[e^Q - 1\right],$ $Q = B_1 \operatorname{tr}(\mathbf{E}) + B_2 E_{ff}^2 + B_3(E_{ss}^2 + E_{nn}^2 + 2E_{sn}^2) + B_4(E_{fs}^2 + E_{fn}^2)$
	Hill et al. (73) $\Psi = A\left[e^{B_1 E_{11}^2} + e^{B_2 E_{22}^2} + e^{B_3 E_{11} E_{22}} - 3\right]$	
Orthotropic	Hunter et al. (74) $\Psi = \sum_{i,j} A_{ij} E_{ij}^2 / \left\| B_{ij} - |E_{ij}| \right\|^{C_{ij}} \left(i, j = f, s, n; A_{ij} = A_{ji}; B_{ij} = B_{ji}; C_{ij} = C_{ji}\right)$	
	Costa et al. (75) $\Psi = A[e^Q - 1],$ $Q = \sum_{i,j} B_{ij} E_{ij}^2 \left(i, j = f, s, n; B_{ij} = B_{ji}\right)$	
	Schmid et al. (76) $\Psi = \sum_{i,j} A_{ij}[e^{B_{ij} E_{ij}^2} - 1], \left(i, j = f, s, n; A_{ij} = A_{ji}; B_{ij} = B_{ji}\right)$	

[a]A, B, …, H are biomechanical material constants.

Table 2

Summary of structural constitutive models for passive behavior of myocardium[a]

General form for structurally informed models $W = W^g(I_1) + W^f(\mathbf{E}, \mathbf{N}, \mathbf{R}, \mathbf{D})$	Reference
$\psi^g = 0$, $\psi^f = \psi^m + \psi^c$ $\Psi^m = \int_{-\pi/24}^{\pi/24} R_1 w_1^* d\alpha$, $\Psi^c = \int_{-\pi/24}^{-\pi/24} \int_0^{2\pi} \int_0^{\pi} R_2 w_2 J d\phi \, d\theta \, d\alpha$ $w_k = A_k \epsilon_k^2$, $D_k(x) = 1/(\sqrt{2\pi}\sigma_k) e^{-(m_k - x)/2\sigma_k^2}$, $k = 1, 2$, ϵ is the fiber true strain	Horowitz et al. (87)
$\Psi^g = A[e^{B(I_1 - 3)} - 1]$, $\Psi^f = \int_{R_i}^{R_o} w \, dR$ $w = C[\epsilon^{D(\sqrt{I^f} - 1)^2} - 1]$	Humphrey & Yin (80)
$\psi^g = 0$, $\Psi^f = \int_{-\pi/2}^{\pi/2} R_1 w_1 \, d\theta + \int_0^{\pi} R_2 w_2 \, d\theta + \int_0^{\pi} \int_0^{\pi/2} R_3 w_3 \, d\theta \, d\phi$ $w_k = A_k \epsilon^2/(B - \epsilon)^C$, $k = 1, 2, 3$, $\epsilon = (I^f - 1)/2$	Hunter et al. (74)
$\psi^g = \phi^g \, k^g/2 \, (I_1 - 3)$, $\Psi^m = \frac{\phi^m}{H} \int_0^H \int_{-\pi/2}^{\pi/2} R^m(\theta, z) w^m(I^m) d\theta \, dz$, $\Psi^c = \frac{\phi^c}{H} \int_0^H \int_{-\pi/2}^{\pi/2} R^c(\theta, z) w^{*c}(I^c) d\theta \, dz$, $\Psi^i = \frac{\phi^c}{H} \int_0^H \int_{-\pi/2}^{\pi/2} \int_{-\pi/2}^{\pi/2} R^m(\theta^m, z) R^c(\theta^c, z) w^{*i}(I^m, I^c) d\theta^m \, d\theta^c \, dz$, $w^m = \frac{k_1^m}{2 \, k_m^2}[e^{k_2^m(\sqrt{I^m} - 1)^2} - 1]$, $w^{*c} = \frac{k^c}{2}(\sqrt{I^c}/\lambda_c - 1)^2$, $w^{*i} = \frac{k_1^i}{2 \, k_i^2}\{e^{k_2^i(I^m + I^c - 2)} - [k_2^i(I^c/\lambda_c^2 - 1) + 1]e^{k_2^i(I^m - 1)}\}$	Avazmohammadi et al. (88)

[a]The reader is referred to the respective references for additional details on the constants and variables.